Applied Surface Science 604 (2022) 154462

Contents lists available at ScienceDirect

Applied Surface Science

journal homepage: www.elsevier.com/locate/apsusc

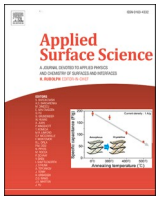

Full Length Article

Parameters controlling octadecyl phosphonic acid self-assembled monolayers on titanium dioxide for anti-fouling biomedical applications

Liana Azizova [a,*], David Morgan [b], Jeff Rowlands [c], Emmanuel Brousseau [c], Tetiana Kulik [d], Borys Palianytsia [d], Jason Peter Mansell [e], James Birchall [f], Thomas Wilkinson [g], Alastair Sloan [h], Wayne Nishio Ayre [a]

[a] School of Dentistry, Cardiff University, United Kingdom
[b] School of Chemistry, Cardiff University, United Kingdom
[c] School of Engineering, Cardiff University, United Kingdom
[d] Chuiko Institute of Surface Chemistry, National Academy of Sciences of Ukraine, Kyiv 03164, Ukraine
[e] Department of Applied Sciences, University of the West of England, United Kingdom
[f] School of Pharmacy and Pharmaceutical Sciences, Cardiff University, United Kingdom
[g] Institute of Life Science, Swansea University, United Kingdom
[h] Melbourne Dental School, University of Melbourne, Australia

ARTICLE INFO

Keywords:
Octadecylphosphonic acid (ODPA)
Self-assembled monolayers (SAMs)
Titanium
Quartz crystal microbalance (QCM)
Atomic force microscopy (AFM)
X-ray photoelectron spectroscopy (XPS)
Water contact angle
Temperature-programmed mass spectrometry (TPD-MS)
Mono- and bidentate attachment

ABSTRACT

Octadecylphosphonic acid (ODPA) self-assembled monolayers (SAMs) have demonstrated potential for deterring bacterial attachment to titanium, however the coating process is time consuming and uses toxic solvents. In this study, ODPA SAM quantity, quality, and structure were evaluated on titanium quartz crystal microbalance (QCM) sensors by varying solvent type (anisole or cyclopentyl methyl ether (CPME), environmentally friendly non-polar solvents); ODPA concentration (0.5 mM or 1 mM); and temperature (21 °C or 60 °C). Surfaces were characterised using QCM frequency and dissipation measurements and Sauerbrey mass calculations; X-ray photoelectron spectroscopy; water contact angle measurements; and temperature-programmed desorption mass spectrometry (TPD-MS). Anti-fouling ability was established against Staphylococcus aureus. Incubation in 0.5 mM ODPA in CPME at 21 °C rapidly formed uniform rigid ODPA SAMs as demonstrated by high Sauerbrey mass (≈285-290 ng/cm^2), viscoelastic modelling, high atomic percentage surface phosphorus (1.1 %) and high water contact angles (117.6 ± 2.5°), consistent across the entire sample surface. High temperatures or the use of anisole resulted in suspected multilayer formation, which reduced bacterial attachment. TPD-MS confirmed covalent bonding of ODPA SAMs on TiO_2 at ≈ 110–120 °C and thermal stability below 300 °C. This study demonstrates the key parameters that control ODPA SAM formation on titanium and their future potential for biomedical applications.

1. Introduction

Titanium and its alloys are widely used for biomedical applications due to the naturally forming oxide layer that provides beneficial biocompatible, corrosion resistant and osteoconductive properties [1,2]. Furthermore, the formation of hydroxyl groups (Ti-OH) on titanium surfaces provide additional catalytical and adsorption properties [3]. Researchers have attempted to further enhance these properties as well as cell adhesion and proliferation capability, through surface modification approaches [4]. An example of such an approach is in the formation of self-assembled monolayers (SAMs), which have been used to bind biomolecules to promote cell differentiation and functional tissue formation [5] as well as in the construction of biosensors, optoelectronics and semiconductor technologies [6].

The most widely used self-assembled monolayers (SAMs) for functionalisation are thiols on metals (gold, silver) and silanes on oxide surfaces. Thiols give uniform and hydrolytically stable films on surfaces however, the major drawback of thiol-based SAMs is a susceptibility to oxidisation that compromise their long-term stability [7]. Organosilane SAMs form by hydrolysis of the labile groups, condensation of oligomers

* Corresponding author at: School of Dentistry, Cardiff University, Heath Park, Cardiff, United Kingdom.
E-mail address: AzizovaL@cardiff.ac.uk (L. Azizova).

https://doi.org/10.1016/j.apsusc.2022.154462
Received 30 March 2022; Received in revised form 18 July 2022; Accepted 2 August 2022
Available online 6 August 2022

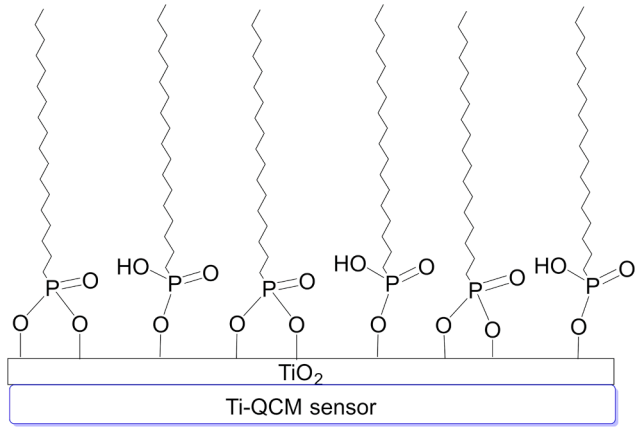

Fig. 1. Schematic representation of octadecylphosphonic acid (ODPA) self-assembled monolayers (SAMs) on the surface of Ti-QCM sensors.

and hydrogen bonding with surface hydroxyl groups resulting in the formation of covalent bonds during curing [8]. The amount of water present in solution during functionalization is a key factor influencing the quality of the monolayer in order to avoid premature polymerization of the silane and multilayer adsorption [9]. Phosphonic acid SAMs produce a more robust film than the previously discussed compounds due to their greater hydrolytic stability. Octadecylphosphonic acid (ODPA) SAMs in particular, have been used to modify surfaces of different oxides, such as titanium [10], copper [11], aluminium [12,13], cobalt-chromium alloy [14] and have demonstrated additional biomedical benefits in encouraging osseointegration and preventing bacterial colonisation [8,10].

A major constraint for the industrial application of ODPA SAMs however is the time required to develop well-ordered layers on the surface. Usually, ODPA SAMs are formed after incubation of the substrate in a solution of ODPA over several hours using polar solvents [15]. It has been previously reported for indium tin oxide surfaces however that the type of solvent has a powerful influence on the quality and formation of ODPA SAMs [16]. Importantly, for titanium modification, differences between water and toluene have been shown to affect not only the binding mechanism of propylphosphonic acid and the close packing of the molecules but the solvent of choice has also been shown to influence the impact of other processing conditions, such as temperature and ODPA concentration, on the successful development of a SAM [17]. Nie and co-authors discovered that well-ordered SAMs of ODPA only formed on the surface of silicon wafers and aluminium films when using non-polar solvents whilst use of polar solvents resulted in low quality SAMs [18–21]. The researchers also showed that full coverage and well-ordered SAMs of ODPA were formed specifically in non-polar solvents with dielectric constants between 3 and 5 [20]. Interestingly, the use of these specific non-polar solvents significantly decreased deposition times from days and hours to minutes and seconds [20,21]. Furthermore the ability to form SAMs using environmentally friendly solvents such as anisole (dielectric constant of 4.3) has also been demonstrated for aluminium films [18].

Thermal treatment following ODPA deposition has also been shown to play an important role in enhancing the stability of the SAMs formed on titanium dioxide (TiO_2) [22]. It has been suggested that thermal treatment transforms hydrogen-bonded phosphonates on TiO_2 into covalent bonded species [22,23]. Although this approach is widely accepted and used, the time and temperature required to achieve covalent conversion is unclear. Gawalt and co-authors achieved stable ODPA SAMs on titanium by heating to 120 °C for 18 h [22], whilst Chen showed that heating ODPA SAMs on aluminium to 150 °C for 15 min is sufficient [18].

Despite the vast number of studies on ODPA SAMs on different surfaces, there are no systematic studies that explore parameters, such as green solvent type (within the dielectric constants of 3 and 5), ODPA concentration and temperature, on the quality of ODPA SAMs formed on

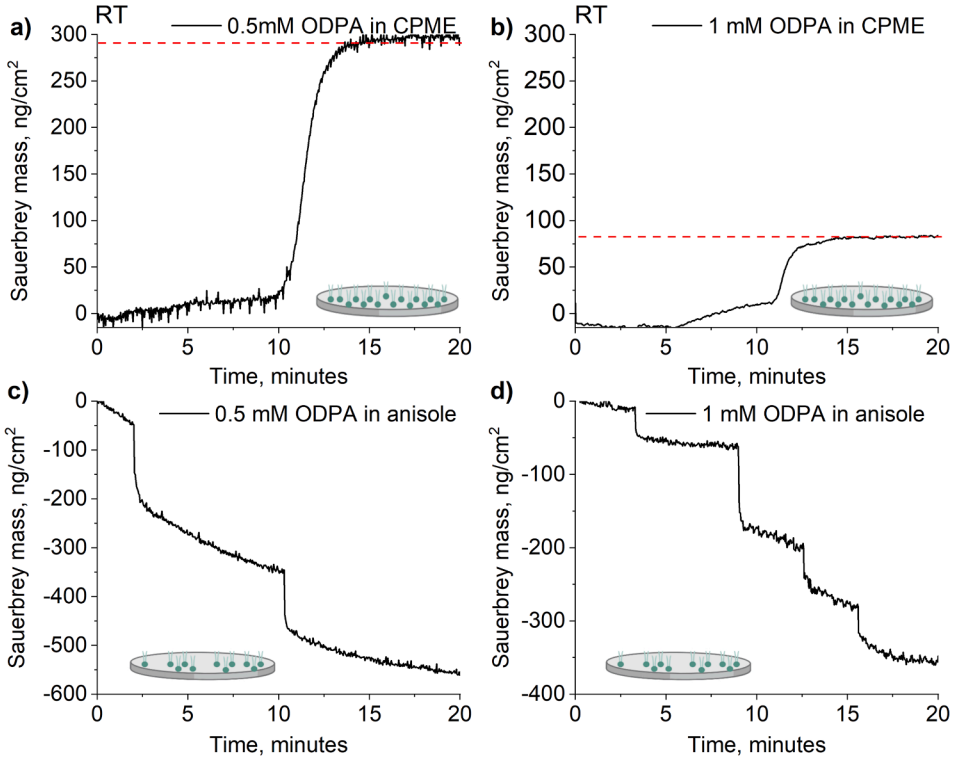

Fig. 2. Quartz crystal microbalance (QCM) Sauerbrey mass measurements of Ti-QCM sensors at RT subjected to ODPA deposition using: (a) 0.5 mM ODPA in CPME; (b) 1 mM ODPA in CPME; (c) 0.5 mM ODPA in anisole; (d) 1 mM ODPA in anisole. The red dashed line indicates the formation of a packed monolayer. (For interpretation of the references to colour in this figure legend, the reader is referred to the web version of this article.)

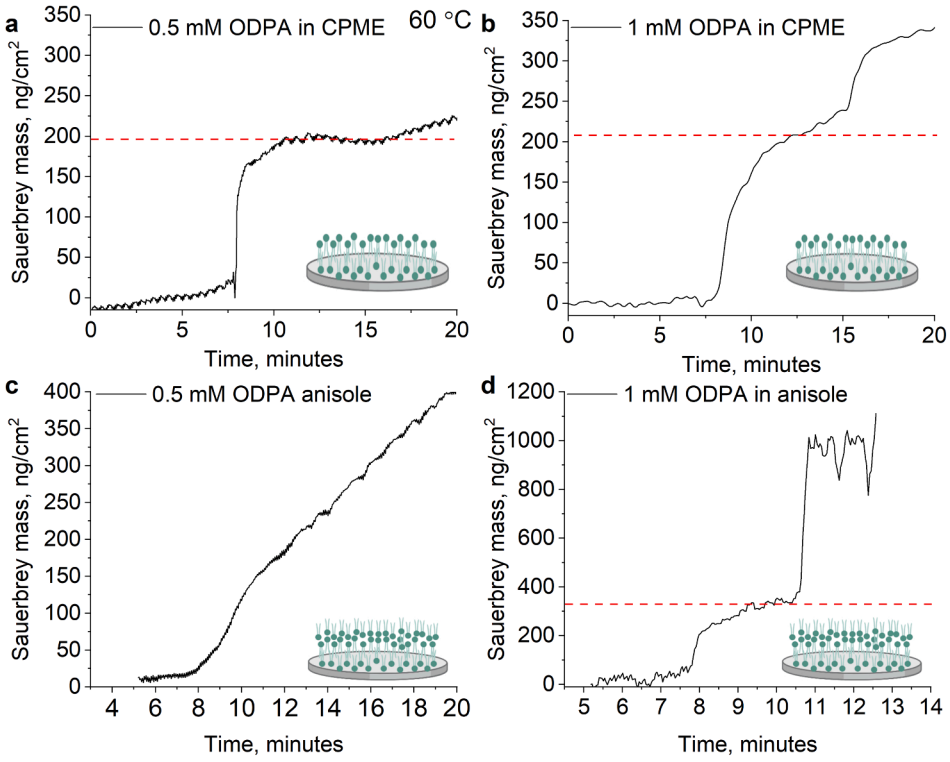

Fig. 3. Quartz crystal microbalance (QCM) – Sauerbrey mass measurements were conducted to describe octadecylphosphonic acid (ODPA) deposition on the surface of Ti-QCM sensor at 60 ℃. The following solutions are used for ODPA deposition: (a) 0.5 mM ODPA in CPME; (b) 1 mM ODPA in CPME; (c) 0.5 mM ODPA in anisole; (d) 1 mM ODPA in anisole. The red dashed line indicates the formation of a packed monolayer. (For interpretation of the references to colour in this figure legend, the reader is referred to the web version of this article.)

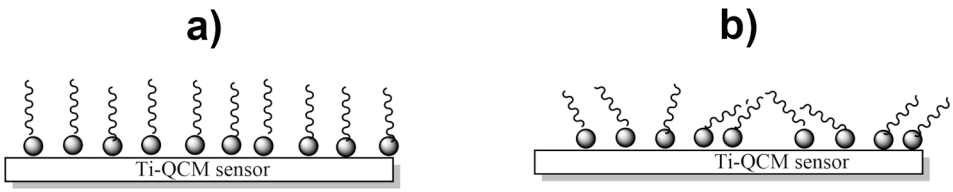

Fig. 4. A schematic presentation of (a) rigid well-ordered layer and (b) less-ordered viscoelastic layer of octadecylphosphonic acid (ODPA) on the surface of Ti-QCM sensors.

TiO_2, a material widely employed for biomedical applications. The aim of this work was to therefore select the optimal surface modification conditions (solvent, concentration and temperature) that result in well-ordered ODPA SAMs on TiO_2 surfaces whilst minimizing processing time for industrial scalability and biomedical applications. The ODPA SAMs formed on TiO_2 were characterized using quartz crystal microbalance (QCM), X-ray photoelectron spectroscopy (XPS), water contact angle measurements, atomic force microscopy (AFM) and temperature-programmed desorption mass spectrometry (TPD-MS). Modified TiO_2 surfaces were also tested for their ability to inhibit *Staphylococcus aureus* colonisation (widely implicated in medical implant infections) to highlight potential biomedical applications.

2. Materials and methods

2.1. Materials

AT cut, 14 mm TiO_2-coated QCM sensors (Ti-QCM, Ti/Au metallization with a TiO_2 coating and resonant frequency of 5 MHz) were purchased from Microvacuum Ltd (Budapest, Hungary). *n*-octadecylphosphonic acid (ODPA; $CH_3(CH_2)_{17}PO(OH)_2$), propanol-2, cyclopentyl methyl ether (CPME; 99.9% pure) and anisole (99% pure) were purchased from Fisher Scientific (Loughborough, UK).

2.2. Ti-QCM sensor cleaning

Prior to modification with ODPA, Ti-QCM sensors were briefly immersed in ultrapure water (18 MΩ; MilliQ) and then dipped in propanol-2 to eliminate any surface contamination. Subsequently, sensors were blown dry with a nitrogen (N_2) gas stream. Finally, Ti-QCM sensors were cleaned using UV/ozone cleaning for 15 min (Ossila UV Ozone Cleaner, Sheffield, UK) and immediately mounted on the QCM flow cell.

2.3. Surface modification and QCM measurements

A QCM system with impedance measurement and dissipation (QCM-I, MicroVacuum Ltd, Budapest, Hungary) was used to study adsorption kinetics of ODPA on TiO_2. The Ti-QCM sensors were modified using the following combinations of conditions: 0.5 mM or 1 mM ODPA concentrations in either anisole or CPME at either at room temperature (RT, 21 °C) or 60 °C. These solvents were selected due to their dielectric constants and "green" status. The concentrations of ODPA were chosen following initial solubility screening in the selected solvents and the temperatures were selected to avoid excess solvent evaporation during use. Solutions of ODPA in solvents were prepared by dissolving ODPA powder in CPME and anisole. Before injection with the ODPA-containing solvent, the QCM sensors were stabilized with the washing buffer (solvent) for 15 min at a flow rate of 100 μL/min using a

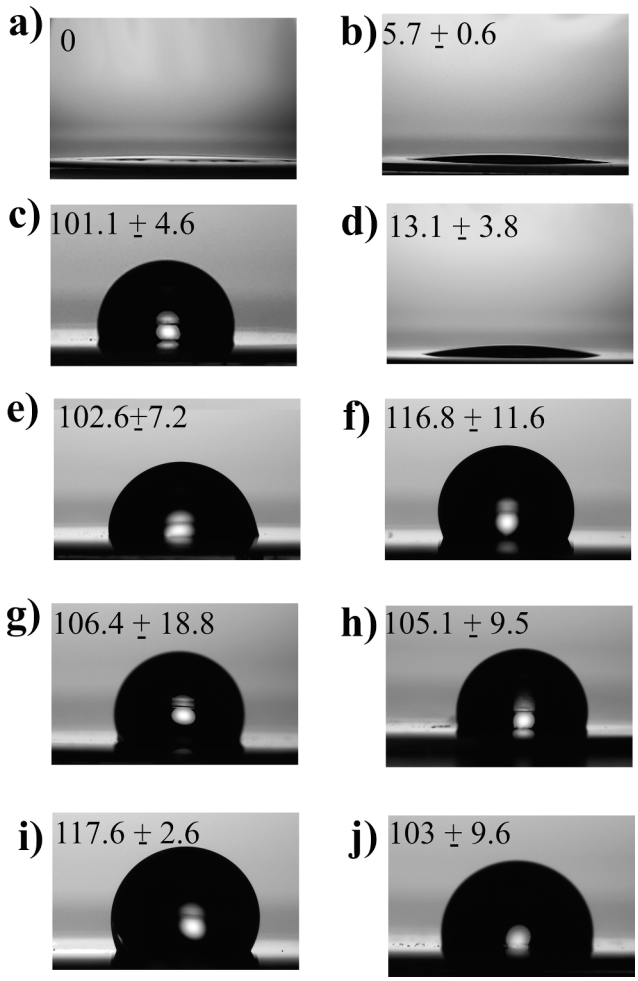

Fig. 5. Representative water contact angles on the surface of modified Ti-QCM sensors. (**a**) Ti-QCM sensor immediately after UV/ozone cleaning; (**b**) Ti-QCM sensor 10 min after UV/ozone cleaning; (**c**) 0.5 mM ODPA in anisole at RT; (**d**) 1 mM ODPA in anisole at RT; (**e**) 0.5 mM ODPA in CPME at 60 °C; (**f**) 1 mM ODPA in CPME at 60 °C; (**g**) 0.5 mM ODPA in anisole at 60 °C; (**h**) 1 mM ODPA in anisole at 60 °C and (**i**) 0.5 mM ODPA in CPME at RT (**j**) 1 mM ODPA in CPME at RT.

peristaltic pump (Ismatec RS232 IN). ODPA containing solutions were then injected through the QCM cell at a flow rate of 100 μL/min using a Rheodyne MXP injection system with a semiautomatic switching valve (MXP9960-000). During the experiment, solutions were kept at RT or at 60 °C using a waterbath (Fisher Scientific Isotemp GPD 02) and the QCM cell was kept at the corresponding temperature using a high precision built in Peltier driver to avoid temperature drifts (stability of ±0.02° C). Frequency at the 1st, 3rd and 5th overtones and dissipation measurements were collected and Sauerbrey mass [24] was calculated using Biosense software (Microvacuum, Budapest, Hungary). Experiments were terminated 20 min after injection with the ODPA solution.

2.4. Water contact angle measurements

The hydrophobicity of the ODPA-coated Ti-QCM sensors was measured using an Attension Theta Lite Optical Tensiometer (Biolin Scientific, Manchester UK). A sessile 4 μL liquid drop of ultrapure water (18 MΩ) was applied to the surfaces at RT and the water contact angle was recorded for 10 s and analysed using OneAttension software (Biolin Scientific, Manchester, UK). Three measurements were taken across different locations on the Ti-QCM sensors and the average contact angle values calculated. An uncoated Ti-QCM sensor was used as a control.

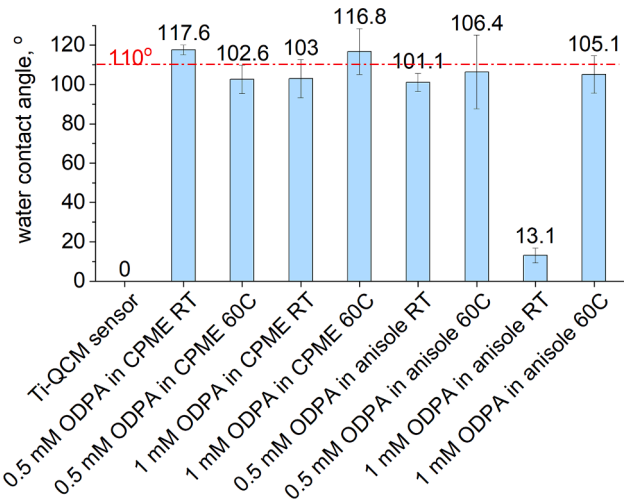

Fig. 6. Average water contact angles on Ti-QCM sensors modified using different solvents, concentrations and temperatures. Red dotted line represents water contact angle value reported for well-ordered SAMs. (For interpretation of the references to colour in this figure legend, the reader is referred to the web version of this article.)

2.5. Atomic force microscopy (AFM)

AFM was used to study the surface morphology and roughness of ODPA-modified Ti-QCM sensors over an area of 2x2 μm^2. High-resolution images were taken at room temperature and atmospheric pressure. A XE-100 AFM system (Park Systems, Mannheim, Germany) was used to image the surface topography. The AFM measurements were performed in non-contact mode using commercial NSG30 probes obtained from NT-MDT (Moscow, Russia). XEP software (Park Systems, Germany) was used for the data acquisition and the Gwyddion software was employed for the post-processing of the AFM data.

2.6. X-ray photoelectron spectroscopy (XPS)

X-ray photoelectron spectroscopy (XPS) data for the ODPA-modified Ti-QCM sensors were collected using a Thermo Fisher Scientific K-alpha$^+$ spectrometer (Loughborough, UK). Samples were analysed using a micro-focused monochromatic Al X-ray source (72 W) using the "400-μm spot" mode, which provides an analysis defining elliptical C-ray spot of 400 × 600 μm. Data was recorded at pass energies of 150 eV for survey scans and 40 eV for high resolution scans with 1 eV and 0.1 eV step sizes respectively. Charge neutralisation of the sample, where required, was achieved using a combination of both low energy electrons and argon ions. Data analysis was performed in CasaXPS v2.3.24 [25] after calibrating the data to the lowest C(1s) component taken to have a value of 285 eV. Quantification was made using a Shirley type background and Scofield cross sections, with an electron energy dependence of −0.6. The XPS spectra were acquired at three different spots on each ODPA-modified Ti-QCM sensors and the bare Ti-QCM sensors as a control. The mean and standard deviations of measurements from three different sample locations were calculated.

2.7. X-ray diffraction (XRD) and temperature-programmed desorption mass spectrometry (TPD-MS)

X-ray diffraction was employed to detect the crystal structure of the Ti-QCM samples to ensure the TiO_2 powder samples required for TPD-MS measurements had similar crystal structures. The surface of Ti-QCM samples were scanned between 10° and 50° (2θ) at a scan speed of 0.020°/s using a Philips PW3830 X-ray generator with a PW1710 Diffractometer control (Philips Research, Eindhoven, Netherlands) and

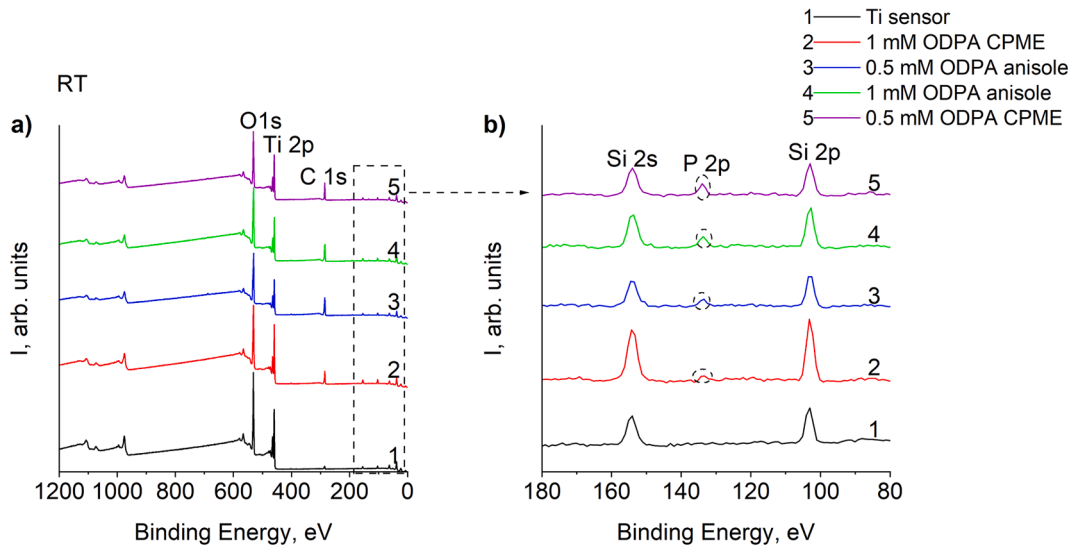

Fig. 7. XPS survey scans in the range (**a**) 0–1200 eV and (**b**) 80–180 eV of bare Ti-QCM (1) and ODPA-films deposited on the surface of Ti-QCM sensor at RT after incubation in the following solutions: 1 mM ODPA in CPME (2); 0.5 mM ODPA in anisole (3); 1 mM ODPA in anisole (4); and 0.5 mM ODPA in CPME (5).

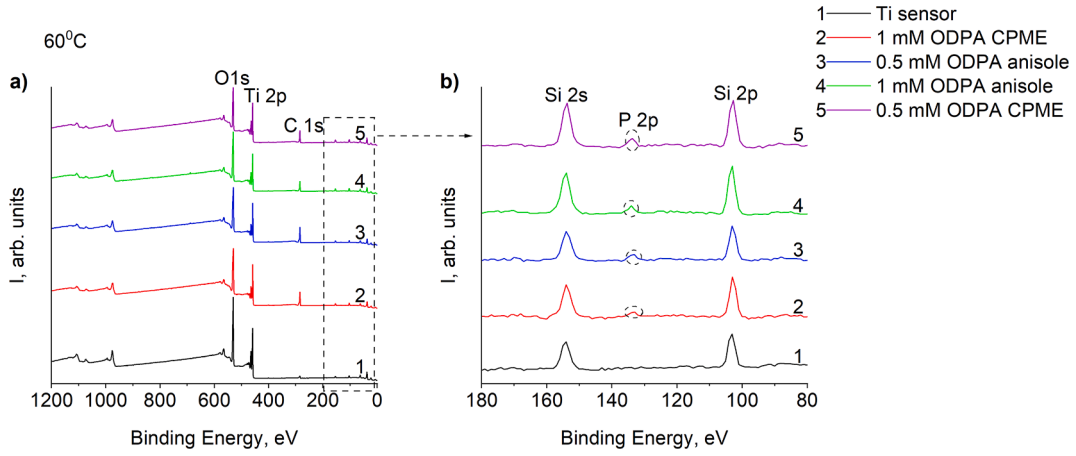

Fig. 8. XPS survey scans in the range **a**) 0–1200 eV and **b**) 80–180 eV of bare Ti-QCM (1) and ODPA-films deposited on the surface of Ti-QCM sensors at 60 °C after incubation in the following solutions: 1 mM ODPA in anisole (2); 0.5 mM ODPA in CPME (3); 1 mM ODPA in CPME (4); and 0.5 mM ODPA in anisole (5).

X'pert Industry v1.1c software (PANalytical B.V., Almelo, Netherlands).

TPD-MS spectra for ODPA, untreated rutile TiO_2, and ODPA-modified rutile TiO_2 powder was collected using a MKh-7304A monopole mass spectrometer (Electron, Sumy, Ukraine) with electron impact ionization. A typical test comprised placing a ~10 mg sample to the bottom of a molybdenum-quartz ampoule, evacuating to ~$5{\cdot}10^{-4}$ Pa at ~20 °C and then heating at 0.17 °C/s from room temperature to ~750 °C. The mass spectra were recorded and analysed using a computer-based data acquisition and processing setup. The TPD-MS procedure and procedure for obtaining kinetic parameters of the thermal reactions in the condensed phase and on the surface of highly dispersed oxides (temperature of maximum desorption rate (T_{max}), the order of the reaction (n), the pre-exponential factor (ν_0), activation energy ($E^{\neq}$), and change of activation entropy ($\Delta S^{\neq}$)) from TPD-MS data has been described in detail earlier [26–32]. 100 mg of TiO_2 was immersed in 0.5 and 1 mM ODPA solution in CPME/anisole and agitated at room temperature for 10 min. After 10 min of shaking, the suspensions were centrifuged for 15 min at 15,000 rpm at RT and the supernatants discarded. The samples were dried in air at room temperature for 24 h before being analysed.

2.8. *Staphylococcus aureus* viability on the surface of ODPA-modified TiO_2

To determine whether specific ODPA structures demonstrated antibacterial properties, 10 mL of tryptone soya broth was inoculated with a single colony of *S. aureus* NCTC 7791 and incubated overnight at 37 °C, 5% CO_2 with shaking. The overnight culture was centrifuged at 5000 g for 5 min and the pellet resuspended in sterile PBS to give an absorbance at 600 nm of 0.08–0.1 (approximately $1x10^7$ CFU/mL). A 1 mL bacterial suspension in PBS containing a $1x10^7$ CFU/mL was applied on the surface of ODPA-modified Ti-QCM sensors and bare Ti-QCM sensors in a 24 well plate. The samples were incubated for 1 h at 37 °C, 5% CO_2. Following incubation, the Ti-QCM sensors were transferred into a sterile 24-well plate and gently washed with 1 mL of 0.85% NaCl to remove non-adherent bacteria. 20 µL of LIVE/DEAD™ BacLight™ Bacterial Viability (Thermofisher Scientific, Paisley, UK, stain containing syto 9 and propidium iodide) was applied to the surface of each of the Ti-QCM sensors. Ti-QCM sensors were covered with a sterile glass coverslip and left at RT for 1 min. *S. aureus* on bare Ti-QCM surfaces were used as live positive controls, whilst dead positive controls consisted of treating *S. aureus* on bare Ti-QCM surfaces with 70 % propanol-2 for 1 h. Three random images of the sensor surface were taken using a Provis AX-70

Table 1
Atomic percent concentration (at.%) of elements obtained from Ti-QCM sensors as determined from Survey spectra.

Conditions/ elements	C 1s	O 1s	Ti 2p	P 2p	Si 2p	N1s	F1s
Ti-QCM sensor	28.2 ± 5.4	52.4 ± 2.2	16.8 ± 1.2	—	1.7 ± 2.1	0.9 ± 0.3	—
Ti-QCM sensor after UV/ ozone cleaning	7.6	65.8	20.4	—	5.5	0.7	—
0.5 mM ODPA CPME RT	31.7 ± 3.2	48.3 ± 2.3	13.2 ± 1.3	1.1 ± 0.3	5 ± 0.4	0.5 ± 0.03	0.31
1 mM ODPA CPME RT	22.2 ± 0.4	55 ± 0.5	14.3 ± 0.7	0.3 ± 0.1	7.7 ± 0.3	0.7 ± 0.1	—
0.5 mM ODPA CPME 60 °C	27.7 ± 4.1	49.9 ± 2.7	12.7 ± 1.3	0.6 ± 0.1	7.2 ± 2.5	0.5 ± 0.1	1.4 ± 0.8
1 mM ODPA CPME 60 °C	23.3 ± 1.6	53.1 ± 0.9	13.1 ± 1.1	0.7 ± 0.1	8.1 ± 0.6	0.8 ± 0.1	0.9 ± 0.2
0.5 mM ODPA anisole RT	34.3 ± 1.7	47.7 ± 1.9	12.4 ± 0.7	0.7 ± 0.1	4.0 ± 0.6	0.8 ± 0.2	0.4 ± 0.1
1 mM ODPA anisole RT	33.1 ± 2.3	45.9 ± 2.3	12.5 ± 0.6	0.8 ± 0.2	5.0 ± 1.1	0.6 ± 0.1	0.3 ± 0.1
0.5 mM ODPA anisole 60 °C	32.3 ± 1.8	49.6 ± 2.7	14.9 ± 2.1	0.6 ± 0.3	2.0 ± 2.8	0.9 ± 0.2	—
1 mM ODPA anisole 60 °C	30 ± 3.2	49.8 ± 1.9	14.0 ± 1.6	0.6 ± 0.1	5.4 ± 0.2	0.7 ± 0.1	—

fluorescent microscope (Olympus, Tokyo, Japan) at 10x, x20 and x40 magnification with emission/excitation wavelengths of 485/530–630 nm respectively and the percentage area coverage quantified as described previously [10].

3. Results and discussion

The aim of this work was to optimise ODPA surface modification conditions (solvent, concentration and temperature) to create well-ordered, scalable SAMs on TiO_2 surfaces for biomedical applications. Previous research has demonstrated that the polarity of solvents play a decisive role in the formation of self-assembled films of ODPA [18,20]. Modification of mica and aluminium by immersion in ODPA solutions in polar solvents requires several hours or even days, whilst full surface coverage using nonpolar solvents with dielectric constants between 3 and 5 can achieve SAMs in seconds [20]. Nonpolar solvents with dielectric constants between 3 and 5 have been proposed to help align ODPA headgroups on the surface and orient them towards hydrophilic moieties on the surface [20]. In the case of TiO_2 and ODPA, the phosphate groups covalently bind to the native oxide layer of titanium (Fig. 1). SAMs of ODPA were rapidly created from nonpolar solvents such as chloroform, trichloroethylene and anisole by spin- and dip-coating techniques [20]. Chen and co-workers [16] concluded that solvent-substrate interactions play a decisive role in the formation of well-ordered SAMs, whilst the nature of the SAM forming molecule has little influence on the quality of the SAMs on the surface.

In order to obtain well-ordered SAMs on the surface, low dielectric constant solvents should be employed, however they must not form complexes with the substrate [16]. Therefore, non-polar solvents such as anisole ($\varepsilon = 4.3$) and cyclopentyl metyl ether (CPME) ($\varepsilon = 4.76$) were employed in this study. Furthermore, both solvents are considered "green" in consideration of environmental impact, with CPME considered a "green" alternative to the conventionally used tetrahydrofuran.

As shown in the QCM Sauerbrey mass data in Fig. 2, monolayer coverage (red dashed line) on the surface of Ti-QCM sensors were achieved in solutions of 0.5 mM ODPA in CPME at RT and 1 mM ODPA in CPME at RT. Interestingly higher amounts of ODPA were deposited on the surface of Ti-QCM sensors when using 0.5 mM ODPA in CPME at RT (≈285-290 ng/cm^2 or 5.13–5.2 × 10^{14} molecules/cm^2) (Fig. 2a) when compared to 1 mM ODPA in CPME at RT (≈80-85 ng/cm^2 or 1.44–1.53 × 10^{14} molecules/cm^2). This corresponds to a molar surface coverage ≈0.84 nmol/cm^2, lower than previously reported (1.18 nmol/cm^2, [33,34]). Monolayer deposition of ODPA on the surface of the Ti-QCM sensor was not detected for 0.5 mM and 1 mM ODPA in anisole at RT as demonstrated by a negative Sauerbrey mass (Fig. 2c, d). Such a signal indicates that molecules on the surface of the Ti-QCM sensor have different spatial organizations, for example formation of multilayers, with variable rigidity as the Sauerbrey mass equation assumes the formation of a uniform rigid film [35].

Multi-layer spatial organisation of ODPA was also observed for Ti-QCM sensors subjected to 0.5 mM and 1 mM solutions of ODPA in CPME (Fig. 3a and b respectively) and 1 mM ODPA in anisole at 60 °C (Fig. 3d). This is demonstrated by a gradual increase of the Sauerbrey mass following initial plateau, likely due to the formation of an additional layer of ODPA on the initial SAM. A negative Sauerbrey mass signal was detected for 0.5 mM ODPA in anisole at 60 °C (Fig. 3c) indicating potential punctual rigid loading [35] (random regions of QCM sensor loading with agglomerates of molecules) as demonstrated in Fig. 4. The Sauerbrey equation is applicable only to rigid, uniform thin films and is calculated based on the change in fundamental frequency (i.e. a decrease in the resonant frequency results in an increase in the Sauerbrey mass). It has been reported in the literature that resonant frequency increases, which result in apparent negative Sauerbrey mass, occurs when a punctual rigid (non-uniform) load is applied to the QCM sensor [36]. Such a situation is likely to arise due to aggregates or potential micelle formation.

Water contact angle measurements were employed to analyse the hydrophobicity of the coated Ti-QCM samples and to assess the uniformity the ODPA film formed and whether bilayer structures were deposited on the Ti-QCM sensors. Superhydrophilic surfaces (water contact angle = 0°) were achieved using UV-ozone cleaning (Fig. 5a) prior to ODPA coating. Water contact angles increased after 10 min in air (≈6°) due to adsorption of airborne organic contaminants (Fig. 5b) [3]. ODPA-modification of Ti-QCM sensors resulted in water contact angles higher than 90°, with the exception of Ti-QCM sensors modified with 1 mM ODPA in anisole at RT, which had a water contact angle of ≈13° (Fig. 5d). This water contact angle suggests limited deposition of ODPA on the Ti-QCM sensor, potentially due to ODPA aggregates or micelles forming at concentrations of 1 mM ODPA in anisole at RT. According to literature, water contact angles for highly ordered SAMs of ODPA on TiO_2 are usually above 110°, in line with the values obtained in this study [15]. These water contact angles were obtained by researchers modifying substrates with ODPA using polar solvents for prolonged incubation periods (i.e. 48 h). Water contact angles greater than 110° were obtained for Ti-QCM sensors modified with 0.5 mM ODPA in CPME at RT and 1 mM ODPA in CPME at 60 °C (Fig. 6). Ti-QCM sensors modified with 1 mM ODPA in anisole at 60 °C showed water contact angles equal to ≈105° (Fig. 6). It was reported that water contact angles for aluminium modified from 1 mM ODPA in anisole at 60 °C reached up to 120° [18]. The lower than reported water contact angle on Ti-QCM sensors modified with 1 mM ODPA in anisole at 60 °C suggests that the ODPA film formed may have defects or uneven surface coverage was obtained. Kanta and co-authors studied formation of ODPA films on the surface of amorphous TiO_2 and found that water contact angles reached 110° after 16 h without further increases even after several days immersion at concentrations of 0.2 mM ODPA in THF [15]. Similar values for other phosphonic acid SAMs on titanium have been obtained by other researchers (113.7 ± 1.9°) [37]. Contact angle values of ≥110° are also typical for well-defined alkyl phosphate SAMs [38] studied on tantalum(V) oxide films [39]. Static contact angles for highly

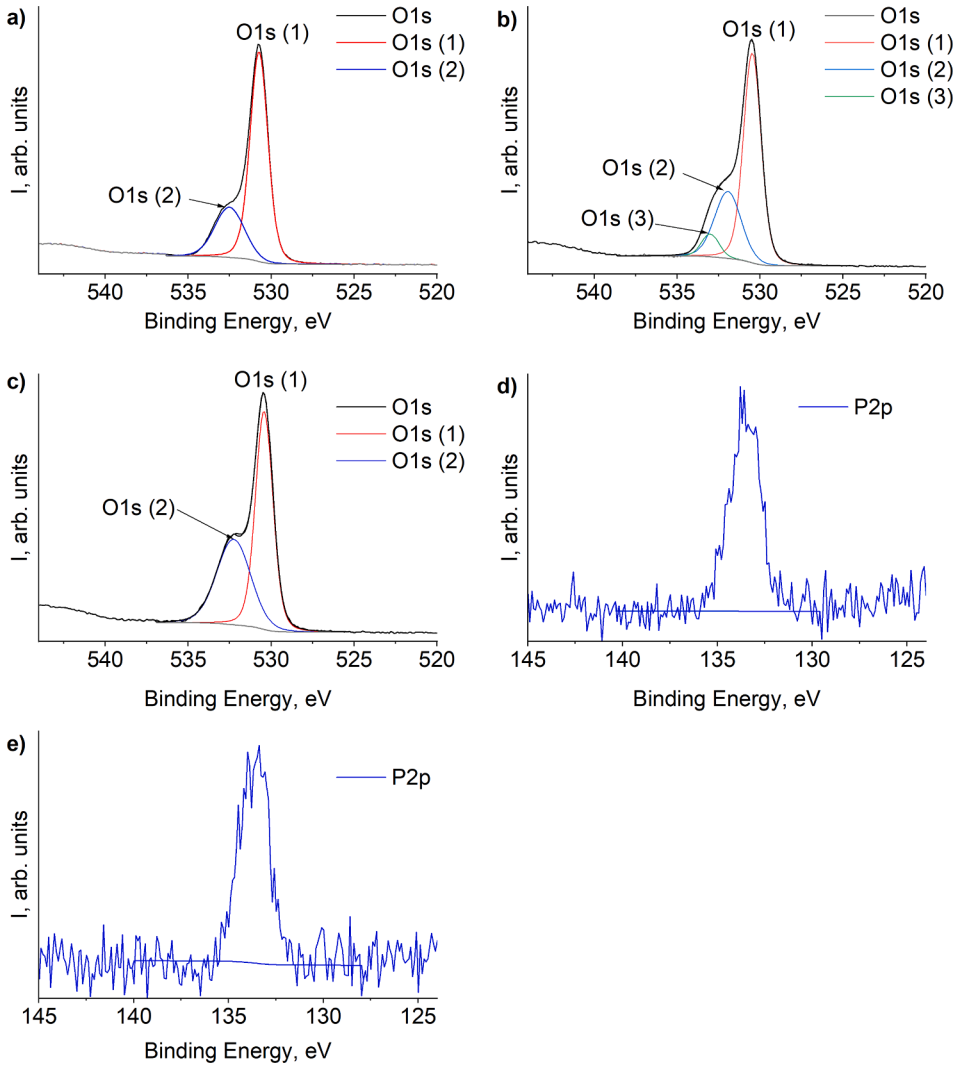

Fig. 9. The O1s XPS spectra of (**a**) bare Ti-QCM sensor after UV/ozone cleaning, (**b**) ODPA/Ti-QCM sensor after modification in 0.5 mM ODPA CPME at RT, (**c**) ODPA/Ti-QCM sensor after modification in 1 mM ODPA anisole at RT. The P2p XPS spectra of (**d**) ODPA/Ti-QCM sensor after modification in 0.5 mM ODPA CPME at RT and (**e**) ODPA/Ti-QCM sensor after modification in 1 mM ODPA anisole at RT.

Table 2
Atomic percent concentration (at.%) of O1s(2) and O1s(3) components fitted in O1s XPS spectrum obtained for Ti-QCM sensors modified with ODPA.

Sample	Atomic percent concentration (at.%) O1s (2) and (Binding energy, eV)	Atomic percent concentration (at.%) O1s (3) and (Binding energy, eV)	Ratio O1s(2)/O1s(3)
0.5 mM ODPA CPME RT	14.2 (531.94)	3.2 (533)	4.4
1 mM ODPA CPME RT	20.2 (532.5)	–	–
0.5 mM ODPA CPME 60 °C	21.0 (532.28)	–	–
1 mM ODPA CPME 60 °C	22.0 (532.25)	3.6 (532.85)	6.1
0.5 mM ODPA anisole RT	19.3 (532.31)	1.6 (533.91)	12.1
1 mM ODPA anisole RT	18.7 (532.25)	–	–
0.5 mM ODPA anisole 60 °C	19.2 (532.46)	–	–
1 mM ODPA anisole 60 °C	20.8 (532.36)	–	–

homogenous, dense ODPA SAMs on indium tin oxide have been reported to be around 104° [16], with similar, lower values also reported for ODPA SAMs on Co–Cr alloys (101.91 ± 0.3°) [14], indicating a minor role of the underlying substrate in lowering the water contact angle.

Water contact angles obtained for Ti-QCM sensors modified with 0.5 mM ODPA in CPME at RT demonstrated even ODPA film formation with a consistent value of 117.6 ± 2.5° across three different regions of the coated Ti-QCM sample (Fig. 5). For the rest of the samples however, water contact angles were highly variable depending on the sensor location, indicating non-uniform layers of ODPA: 13.1 ± 3.8° for 1 mM ODPA in anisole at RT and 105.1 ± 9.5° at 60 °C; 106.4 ± 18.8° for 0.5 mM ODPA in anisole at 60 °C. The water contact angle data supports the QCM data whereby highly ordered and uniform monolayers of ODPA were formed on the surface of Ti-QCM sensors after incubation in 0.5 mM ODPA in CPME at RT.

AFM imaging of the Ti-QCM modified samples failed to show significant differences between non-modified Ti-QCM sensor surfaces and ODPA-modified Ti-QCM sensors due to the roughness of the Ti-QCM sensor (Supplementary Figs. 7S, 8S and Supplementary Table 1S). These findings are in agreement with reported data showing no

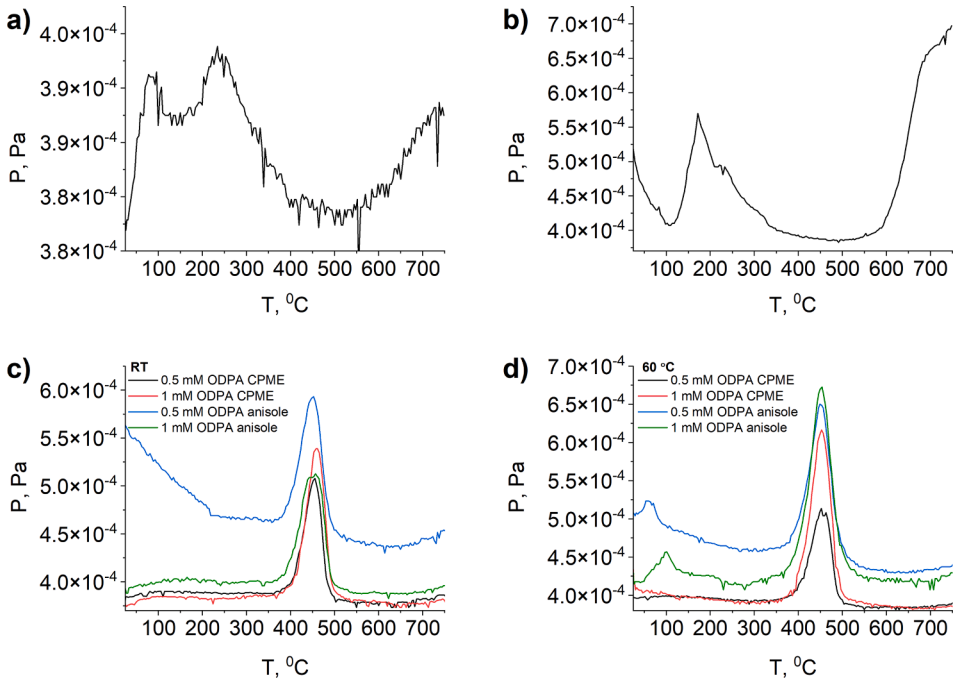

Fig. 10. Vapor pressure of pyrolysis products measured as a function of temperature. (p = f(T)) curves of (a) TiO_2; (b) octadecylphosphonic acid (ODPA) in a pristine state; (c) TiO_2 after incubation in solutions of ODPA at RT; (d) TiO_2 after incubation in solutions of ODPA at 60 °C.

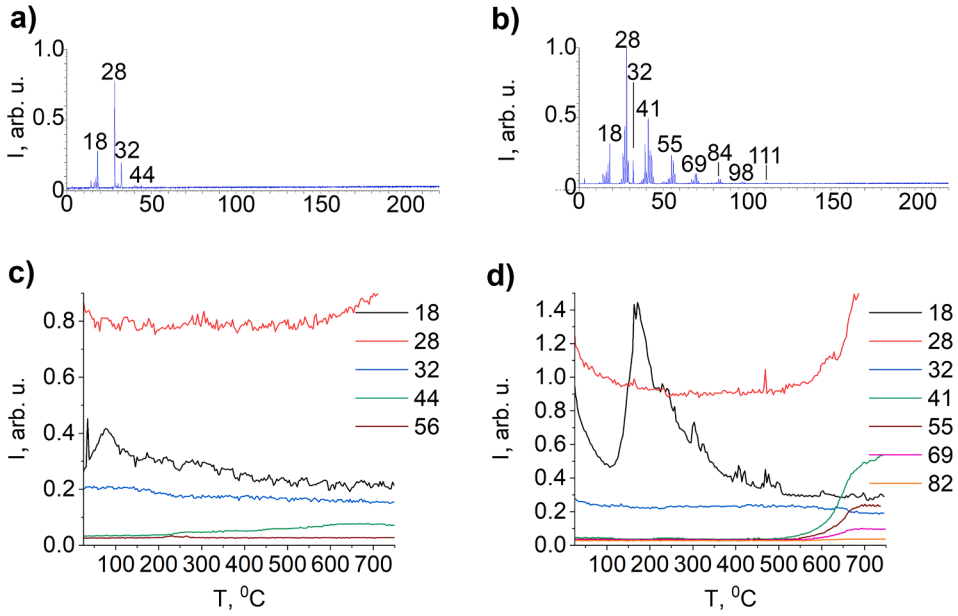

Fig. 11. (a) Mass spectrum of TiO_2 at 150 °C and (b) mass spectra of octadecylphosphonic acid in a pristine state at 700 °C; (c) TPD-curves of TiO_2 in a pristine state; (d) TPD-curves of octadecylphosphonic acid in a pristine state.

morphological changes after ODPA deposition [15]. ODPA films adsorbed on smooth alumina surfaces have been shown to have a height 0.8 nm [40], well below the limit of detection on Ti-QCM sensors. The value of surface roughness for Al samples modified with ODPA was less than 15 nm according to previously published AFM data [41].

The amount of ODPA deposited on the Ti-QCM sensors was quantified using XPS. It was found that C1s and P2p scans showed that the quantity of carbon and phosphorous increased non concomitantly with decreases in Ti and O concentrations (Figs. 7 and 8, Table 1) due to contamination of samples by C—F bond containing compounds. The phosphorus was not detected on the non-modified Ti-QCM sensor surface (control; Table 1), indicating minimal background phosphorous contamination. The highest amount of phosphorus was detected for the Ti-QCM sensor modified by immersion in 0.5 mM ODPA in CPME at RT (1.1 ± 0.3 at%, Fig. 7) and 1 mM ODPA in anisole at RT (0.8 ± 0.2 at% – Fig. 7). The atomic percent concentration of elements obtained from deconvolution of XPS peaks are summarized in Table 1. The highest amount of ODPA evenly distributed on the surface of Ti-QCM sensor was observed when modifying Ti with 0.5 mM ODPA in CPME at RT (1.1 ± 0.3 at%, Fig. 7). This finding coincided with the results of water contact angle measurements and Sauerbrey mass values discussed above.

The O1s XPS spectra of UV/ozone cleaned Ti-QCM sensor are shown

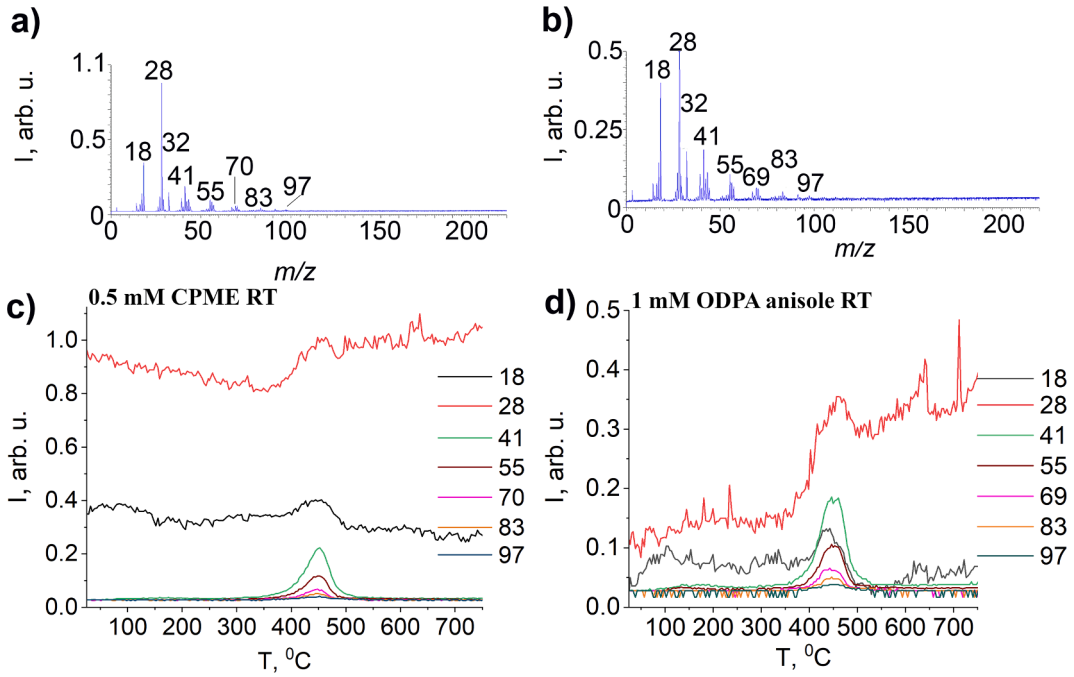

Fig. 12. Mass spectrum at 450 °C of TiO_2 modified in a solution of 0.5 mM octadecylphosphonic acid (ODPA) in CPME RT and (b) mass spectra at 450 °C of TiO_2 modified in a solution of 1 mM octadecylphosphonic acid (ODPA) in anisole RT; (c) TPD-curves of TiO_2 modified in a solution 0.5 mM octadecylphosphonic acid (ODPA) in CPME RT; (d) TPD-curves of TiO_2 modified in a solution 1 mM octadecylphosphonic acid (ODPA) in anisole RT.

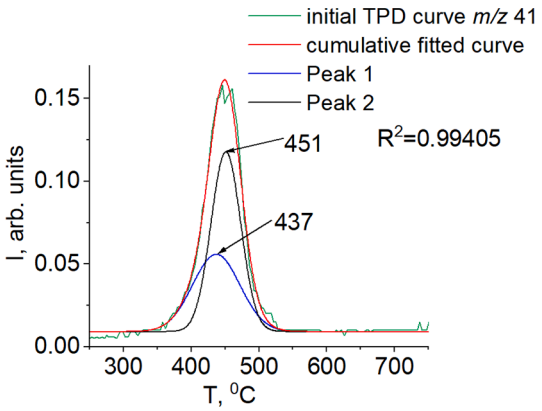

Fig. 13. Deconvolution of the TPD-curve for the ion with *m/z* 41 of TiO_2 modified in the solution of 1 mM octadecylphosphonic acid (ODPA) in anisole RT into separate Gaussians.

in Fig. 9a. The O1s peak in Ti-QCM sensor was fitted to two peaks: (1) O1s(1) at 530.82 was assigned to oxygen in Ti-O bonds in TiO_2; (2) O1s (2) at 532.61 related to the oxygen in Ti—OH bonds [37,42]. The O1s XPS spectra of Ti-QCM sensors modified with 0.5 mM ODPA in CPME at RT (Fig. 9b) were fitted to three peaks. The first peak O1s(1) at 530.47 was assigned to oxygen atoms in TiO_2. The second peak O1s(2) at 531.94 referred to P—O—Ti and P═O. The third peak O1s(3) at 533 is associated with P-OH.

It was reported that the ratio between O1s(2) and O1s(3) peaks can be used to determine the type of interaction of phosphonic acid SAM with the surface [37,43]. The O1s(2) to O1s(3) ratio for unbound phosphonic acid powder was ~0.5 [43]. The covalent bonding of phosphonic acid to the surface increased the ratio to ≥2 due to transformation of some P—O—H bonds (~533 eV) into P—O—Ti bonds (~531.94 eV) [37,43]. Researchers claim that this approach for revealing the binding mechanism of phosphonic acid SAM to the surface is suitable for phosphonic acid monolayers terminated with —CH_3 groups like ODPA [37]. The ratio between the second and third component of O1s peaks was reported to be ~3.4 for hexadecylphosphonic acid on Ti-Nb alloy [43] and to be ~3.2 for dodecylphosphonic acid on Ti [37]. The O1s(2): O1s(3) ratio for Ti-QCM modified with 0.5 mM ODPA CPME RT was ~4.4 (Table 2). This ratio is greater than those reported in the literature and suggests that covalent binding of ODPA to the Ti-QCM sensor took place. Zorn and colleagues suggested that the oxygen signal (531.9/533) ratio of 2:1 would be expected in the case of monodentate modes of attachment when ODPA molecules attach to the surface via one P—O—Ti bond [43]. A ratio >2 demonstrates that phosphonic acid molecules attach to the surface via two P—O—Ti interactions and no P—OH interactions (bidentate configuration) [43]. This bidentate anchoring of ODPA molecules to the surface provides SAM stability. These observations confirm the successful modification of Ti-QCM sensor surfaces with ODPA and are in agreement with previously reported data [37,41].

The further evaluate the robustness and binding mechanisms of the ODPA SAMs, TPD-MS was employed. TiO_2 powder in the form of rutile was used for this measurement as XRD scans revealed that rutile TiO_2 was present on the surface of the bare Ti-QCM (Supplementary Fig. 9S). TiO_2 was modified at RT and at 60 °C by immersion in the following solutions: 0.5 mM and 1 mM ODPA in CPME; and 0.5 mM ODPA and 1 mM ODPA in anisole. The obtained p = f(T) curves and TPD-curves of ODPA-modified TiO_2 were compared with spectra of pristine ODPA and TiO_2. Analysis of vapor pressure of decomposition products measured as a function of temperature curves (the p = f(T)) of pristine TiO_2 (Fig. 10a) indicates that decomposition occurs in three main stages: at T_{max} ≈80 °C, desorption of adsorbed water (*m/z* 18) and carbonaceous contaminants takes place (*m/z* 56 (C_4H_8), 44 (CO_2), 32 (MeOH), 28 (CO)) (Fig. 11a, c); at T_{max} ≈ 250 °C, desorption of chemisorbed substances takes place; and at T_{max} ≈ 750 °C, surface dehydroxylation takes place. Thermal treatment of TiO_2 results in dihydroxylation of titanols (Ti-OH) and the formation of titanoxanes (Ti—O—Ti) [3]. The surface becomes entirely dehydroxylated at temperatures greater than 500 °C [3]. The obtained p = f(T) curves revealed that thermolysis of ODPA in a pristine state occurs in two main stages (Fig. 10b): dehydration during the first stage at T_{max} ≈ 200 °C and decomposition of hydrocarbon chains at T_{max}

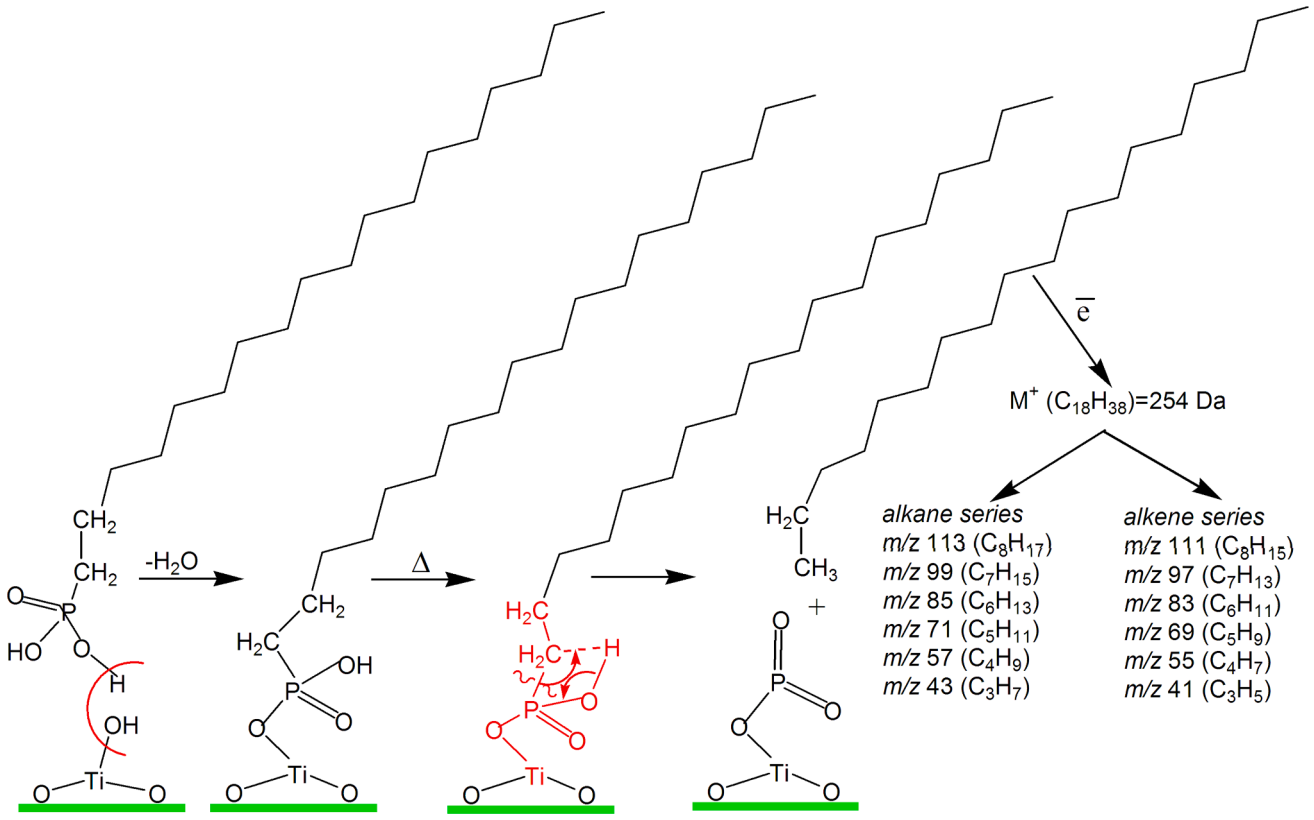

Scheme 1. The possible mechanism of ODPA decomposition on titania surfaces via alkane formation.

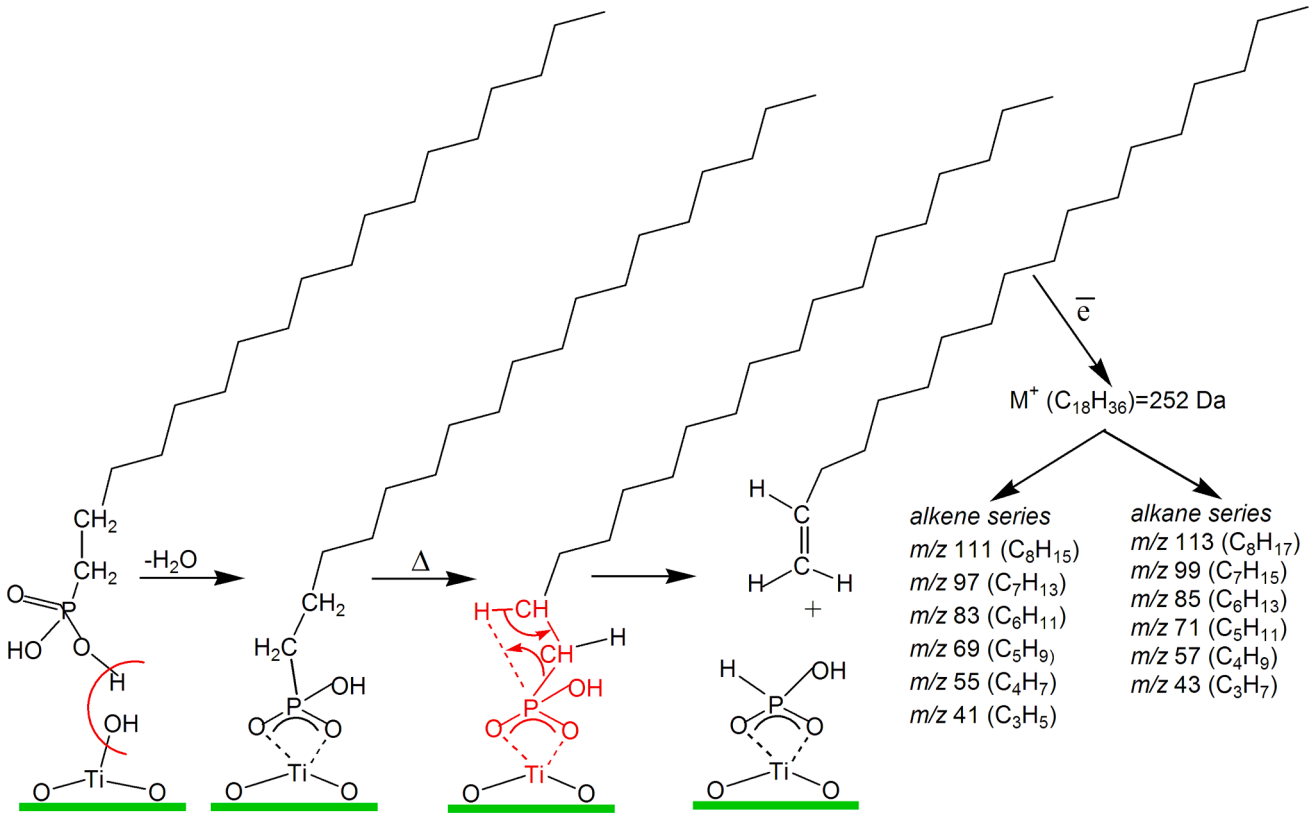

Scheme 2. The possible mechanism of ODPA decomposition on titania surfaces via alkene formation.

Table 3
Kinetic parameters (temperature of the maximum desorption rate T_{max}, reaction order n, activation energy $E^{\neq}$, pre-exponential factor ν_0, and activation entropy $\Delta S^{\neq}$) and peak intensities (I) of ODPA decomposition on TiO_2 obtained after incubation in solutions of 0.5 mM ODPA CPME at RT and 1 mM ODPA anisole at RT.

m/z	*I*, a.u.	T_{max}, °C	*n*	$E^{\neq}$, kJ·mol^{-1}	ν_0, s^{-1}	$\Delta S^{\neq}$, cal·K^{-1} · mol^{-1}	R^{2*}
0.5 mM ODPA CPME RT							
P/T	5.10x10^{-4}	455	1	227	1.71×10^{14}	4.78	0.998
18	0.402	454	1	232	5.21×10^{14}	7.17	0.943
41	0.220	451	1	226	1.27×10^{14}	4.3	0.985
42	0.102	448	1	218	3.53×10^{13}	1.7	0.991
43	0.117	448	1	215	3.19×10^{13}	1.4	0.988
55	0.117	451	1	216	2.75×10^{13}	1.2	0.962
56	0.099	448	1	212	1.74×10^{13}	0.2	0.989
69	0.068	452	1	215	2.47×10^{13}	0.96	0.967
83	0.052	449	1	214	1.71×10^{13}	0.2	0.960
97	0.041	451	1	216	2.66×10^{13}	1.2	0.915
1 mM ODPA anisole RT							
P/T	5.13x10^{-4}	440/455	1	229	2.30×10^{14}	5.5	0.966
18	0.407	442	1	209	9.83×10^{12}	2.9	0.907
41	0.185/0.184	440/455	1	229	1.81×10^{14}	5.0	0.967
43	0.116	439	1	217	3.90×10^{14}	1.9	0.991
55	0.103	455	1	232	3.60×10^{14}	6.2	0.980
69	0.065	449	1	227	1.89×10^{14}	5.0	0.982
83	0.00	447	1	228	1.72×10^{14}	4.8	0.950

*R^2– Coefficient of determination.

≈ 750 °C during the second stage (Fig. 11b, d). According to p = f(T) curves, the thermolysis of TiO_2 modified by ODPA at RT (Fig. 10c) and TiO_2 incubated in ODPA solution in CPME at 60 °C (Fig. 10d) occurs in one stage, while it results in two stages for samples treated with anisole at 60 °C (Fig. 10d): at T_{max} ≈ 100 °C and T_{max} ≈ 450 °C. The main gaseous products produced at the first stage of thermolysis at T_{max} ≈ 100 °C are CO (*m/z* 28) and H_2O (*m/z* 18) (Fig. 12 c, d). Therefore, it can be suggested that samples of titania modified by ODPA be annealed at ~110 –120 °C as water desorption takes place at T_{max} ≈ 110 °C. The decomposition of ODPA molecules chemisorbed on the surface of titania during the second stage of thermolysis begins at 350 °C with maximum at T_{max} ≈ 450 °C (Fig. 10c, d). It is therefore safe to anneal samples of titania modified with ODPA on the surface up to 300 °C in a vacuum. Chen and co-authors found that ODPA on alumina in air can be annealed up to 200 °C as oxidation of the hydrocarbon chains of ODPA by oxygen takes place at higher temperatures [18]. The same pattern was observed for thermal transformation of organosilane SAMs on the surface of TiO_2: there was no weight loss in a nitrogen atmosphere for organosilanes on the surface of TiO_2 until 300 °C [44]. Kanta and co-authors showed that water contact angles of ODPA SAMs supported on TiO_2 obtained from THF decreased to 0° after thermal treatment above 350 °C, indicating complete decomposition of ODPA from the surface of TiO_2 [15]. Another study showed that ODPA SAMs were thermally stable on the surface of alumina up to 500 °C [45].

The fragmentation of ODPA on the surface of titania during the second stage of thermolysis reveals a pattern similar to unbranched alkanes and alkenes (Fig. 12). Therefore, TPD-curves for ions with *m/z* 41, 55, 69, 83, 97 were observed in the spectra (Fig. 12c, d). The most intensive peak on the TPD-curves was for the ion with *m/z* 41.

Interestingly, splitting of the ODPA decomposition peak on titania at T_{max} ≈ 450 °C was detected on p = f(T) (Fig. 10) and TPD-curves for all samples (Fig. 12, Supplementary Figs. 10S–13S). This feature indicates two parallel thermolysis processes (fragmentation of two products) occurring during the second stage of thermal decomposition of ODPA on titania. An especially prominent manifestation of this effect was observed with titania samples modified with 1 mM ODPA anisole at RT (Figs. 10c, 12d). This result is in agreement with the obtained earlier water contact angle values. The greatest decrease in water contact angle was for titania incubated in 1 mM ODPA in anisole at RT (13.1 ± 3.8°). This effect may be related to the spatial organisation of ODPA on the surface of titania: less ordered layers give rise to more obvious peak splitting due to the two types of ODPA binding (monodentate and bidentate). This was previously observed in the decomposition of monodentate complexes and bidentate chelate carboxylate complexes of valeric and ferulic acids) on the surfaces of nanoscale oxides (CeO_2, γ-Al_2O_3, SiO_2, CeO_2/SiO_2, Al_2O_3/SiO_2 and TiO_2/SiO_2) [46–48]. Moreover, the localization of the TPD peaks of the decarboxylation products of ferulic acid on the surfaces of nanosized cerium and aluminium oxides were also within a narrow temperature range.

To study this splitting in more detail, a deconvolution of the TPD-curve of titania modified with 1 mM ODPA anisole RT was performed. The deconvolution of the TPD curve for the ion with *m/z* 41 (base peak ion) into separate Gaussians (Fig. 13) made it possible to determine the temperatures of the maximum decomposition of these products (T_{max} = 437 °C and T_{max} = 451 °C). It should be noted that T_{max} is a significant characteristic of non-isothermal kinetics and is often used for approximate calculations of activation energy [29,30]. T_{max} is directly included in the approximate equation developed by Kislyuk and Rozanov for calculating the activation energy [29,49]. The calculation by the approximate formula gives the following activation energy values for these two parallel reactions: 224 and 228 kJ/mol (n = 1, $\nu_{0\ average} = 2.58\ 10^{14}\ s^{-1}$). Thus, the difference between the activation energies of these two reactions is only 4 kJ mol^{-1}. Such a small difference in activation energies is due to the fact that in both cases, the rate-limiting step is the rupture of the C-P bond (Schemes 1 and 2).

The calculated kinetic parameters for TPD peaks at the second stage of thermolysis (Table 3, Table 2S) showed that this process has kinetics typical to covalent bond decomposition with high values of activation energy and positive values of activation entropy $\Delta S^{\neq} > 0$. Therefore, decomposition of the ODPA chemisorbed complexes proceeds through a disordered transition state.

According to rules of interpretation of fragmentation, the C_nH_{2n-1} and C_nH_{2n} peaks in alkene spectra are more intense than the C_nH_{2n+1} peak of alkanes [50]. In alkane spectra the most prominent peaks are C_nH_{2n+1} [50]. The splitting of the TPD-peak at ~450 °C for the fragment ions is the result of two types of product formation in the close temperature range: alkane (M.r. = 254 Da, *m/z* 113, 111, 97, 83, 69, 55, 41) (Scheme 1) and alkene (M.r. = 252 Da, *m/z* 113, 111, 97, 83, 69, 55, 41) (Scheme 2).

Previous research has demonstrated that phosphonic acid coatings have the capability of reducing bacterial colonisation, in particular *Staphylococcal* species, highly implicated in orthopaedic infections [10,51], however these studies did not fully establish whether SAMs or bilayer structures of phosphonic acids were formed. This is of particular

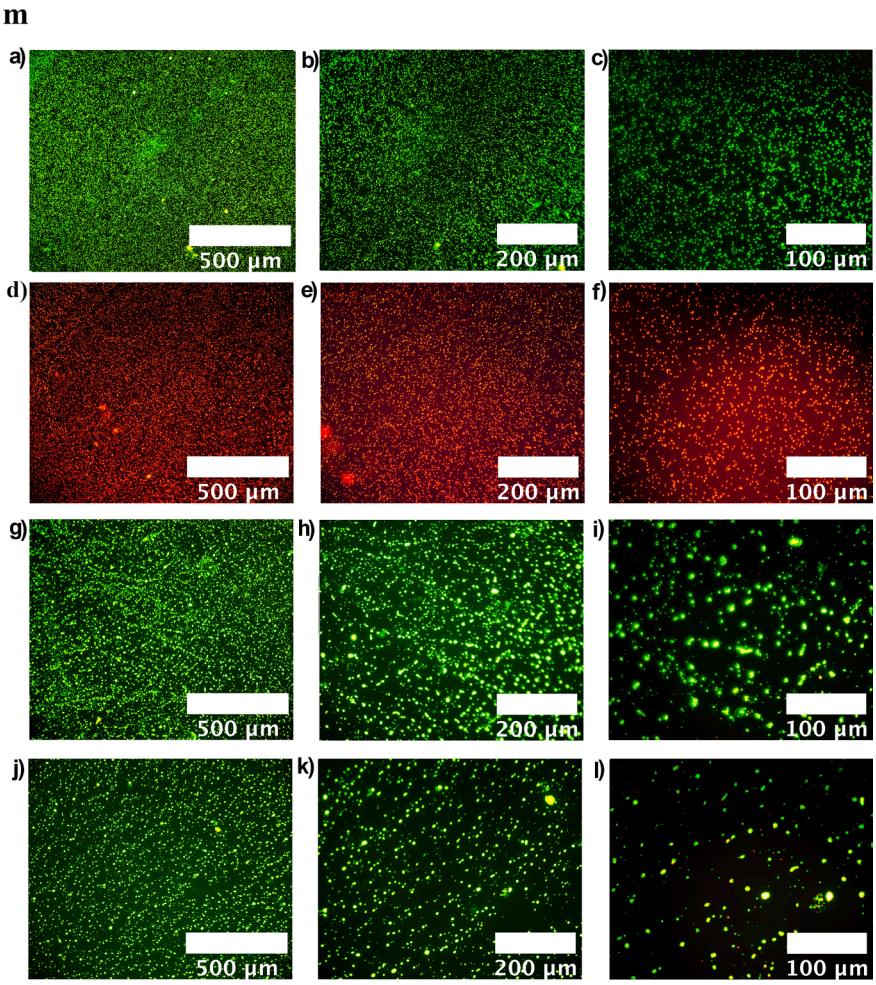

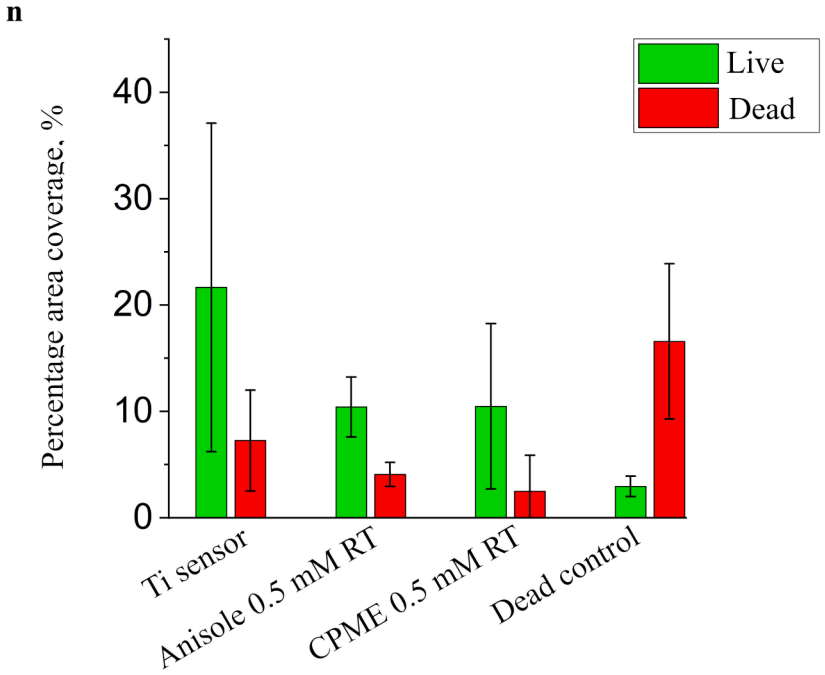

Fig. 14. (a–l). Fluorescent live/dead images of *S. aureus* attached to ODPA-modified Ti-QCM sensors after incubation for 1 h at 37 °C. The green signal is due to the dye SYTO9, indicating live cells whilst the red signal is due to propidium iodide which labels dead cells. The live control at magnification (a) x10; (b) x20; (c) x40; dead control at magnification (d) x10; (e) x20; (f) x40; 0.5 mM ODPA in CPME RT at magnification (g) x10; (h) x20; (i) x40; 0.5 mM ODPA in anisole RT at magnification (j) x10; (k) x20; (l) x40. (**m**). The quantification of *S. aureus* attachment on ODPA-modified Ti-QCM sensors (0.5 mM ODPA anisole RT and 0.5 mM ODPA CPME RT) (**n**). (For interpretation of the references to colour in this figure legend, the reader is referred to the web version of this article.)

importance given both hydrophobicity and surface chemistry plays a critical role in bacterial adherence [52–54]. Wiencek and Fletcher concluded that the number of adherent bacteria are determined by the detachment rate rather than the attachment rate and bacteria are more prone to irreversibly attach with increased CH_3 surface groups (found on the end of the acyl chain of ODPA) [52,55]. Furthermore a separate study by Katsikogianni using two *Staphylococcus epidermidis* strains showed attachment is dependent on terminal functionality, with CH_3 groups resulting in the highest level of attachment, followed by NH_2 and OH terminated surfaces [56]. Following physicochemical characterisation of the ODPA coatings on Ti-QCM sensors, *S. aureus* viability was tested using live/dead staining (Fig. 14). ODPA-modified Ti-QCM sensors did not have any biocidal properties (Fig. 14), in line with previous research that demonstrated phosphonic acids to predominantly prevent adherence [10]. Both the Ti-QCM sensors coated with 0.5 mM ODPA in anisole at RT (Fig. 14j, k, l) and 0.5 mM ODPA in CPME at RT (Fig. 14g, h, i) had visibly reduced *S. aureus* attachment when compared with the uncoated Ti-QCM sensors (Fig. 14a, b, c). Although slight differences in bacterial attachment were observed between the two ODPA conditions, the semi-quantification technique did not demonstrate enhanced anti-fouling properties for the bilayer of ODPA (0.5 mM ODPA in anisole at RT) compared to the monolayer of ODPA (0.5 mM ODPA in anisole at RT). Such differences may be present, however further investigation is required, which is outside the scope of this study.

4. Conclusions.

Modification of titanium biomedical implants with ODPA SAMs have previously demonstrated promising results for deterring bacterial attachment, however existing coating processes are time consuming and require the use of toxic solvents. ODPA deposition on titanium was investigated by incubating Ti-QCM sensors in solutions of 0.5 and 1 mM ODPA in nonpolar solvents, CPME and anisole (dielectric constants of 4.76 and 4.3 respectively) at room temperature and 60 °C. QCM analysis, water contact angle measurements, XPS and AFM revealed that well-ordered uniform ODPA monolayers were rapidly formed in solutions of 0.5 mM ODPA in CPME at RT. The use of anisole and higher temperatures resulted in the formation of non-uniform ODPA monolayers and bilayer structures. In order to covalently bind the coatings to the oxide layer of titanium, TPD-MS demonstrated that temperatures ≈110–120 °C are required for the desorption of water. Temperatures above 300 °C resulted in thermal decomposition of the alkyl chains of ODPA. Although the ODPA coatings did not demonstrate bactericidal activity, there is evidence of anti-fouling properties compared to untreated titanium. In conclusion, this study has established key parameters required for the rapid, robust and uniform formation of an ODPA SAMs on titanium and demonstrates its potential for anti-fouling biomedical applications.

CRediT authorship contribution statement

Liana Azizova: Conceptualization, Methodology, Formal analysis, Investigation, Writing – original draft, Writing – review & editing, Visualization, Project administration. **David Morgan:** Formal analysis, Investigation, Methodology. **Jeff Rowlands:** Investigation. **Emmanuel Brousseau:** Conceptualization, Resources, Writing – review & editing. **Tetiana Kulik:** Methodology, Formal analysis, Investigation. **Borys Palianytsia:** Methodology, Investigation. **Jason Peter Mansell:** Conceptualization, Writing – review & editing. **James Birchall:** Conceptualization, Writing – review & editing. **Thomas Wilkinson:** Conceptualization, Writing – review & editing. **Alastair Sloan:** Conceptualization, Writing – review & editing. **Wayne Nishio Ayre:** Conceptualization, Formal analysis, Writing – original draft, Writing – review & editing, Supervision, Project administration, Funding acquisition.

Declaration of Competing Interest

The authors declare that they have no known competing financial interests or personal relationships that could have appeared to influence the work reported in this paper.

Data availability

Data will be made available on request.

Acknowledgements

This work was supported by the Engineering and Physical Sciences Research Council (EPSRC) grant number EP/T016124/1. XPS data collection was performed at the EPSRC National Facility for XPS (‘HarwellXPS’), operated by Cardiff University and UCL, under contract No. PR16195. We would also like to thank the Armed Forces of Ukraine for providing security to perform this work. For the purpose of open access, the author has applied a CC BY public copyright licence (‘CC BY-ND public copyright licence’) to any Author Accepted Manuscript version arising.

Appendix A. Supplementary material

Supplementary data to this article can be found online at https://doi.org/10.1016/j.apsusc.2022.154462.

References

[1] M. Niinomi, Y. Liu, M. Nakai, H. Liu, H. Li, Biomedical titanium alloys with Young’s moduli close to that of cortical bone, Regen. Biomater. 3 (2016) 173–185.
[2] L. Wang, L. Xie, Y. Lv, L.-C. Zhang, L. Chen, Q. Meng, J. Qu, D. Zhang, W. Lu, Microstructure evolution and superelastic behavior in Ti-35Nb-2Ta-3Zr alloy processed by friction stir processing, Acta Mater. 131 (2017) 499–510.
[3] A. Kanta, R. Sedev, J. Ralston, Thermally- and photoinduced changes in the water wettability of low-surface-area silica and titania, Langmuir 21 (2005) 2400–2407.
[4] L.-C. Zhang, L.-Y. Chen, L. Wang, Surface modification of titanium and titanium alloys: technologies developments, and future interests, Adv. Eng. Mater. 22 (2020) 1901258.
[5] L.S. Tew, J.Y. Ching, S.H. Ngalim, Y.L. Khung, Driving mesenchymal stem cell differentiation from self-assembled monolayers, RSC Adv. 8 (2018) 6551–6564.
[6] M. Singh, N. Kaur, E. Comini, The role of self-assembled monolayers in electronic devices, J. Mater. Chem. C 8 (2020) 3938–3955.
[7] M. Dubey, T. Weidner, L.J. Gamble, D.G. Castner, Structure and order of phosphonic acid-based self-assembled monolayers on Si(100), Langmuir 26 (2010) 14747–14754.
[8] W.N. Ayre, N. Scully, C. Elford, B.A. Evans, W. Rowe, J. Rowlands, R. Mitha, P. Malpas, P. Manti, C. Holt, R. Morgan-Jones, J.C. Birchall, S.P. Denyer, E. sl.,, Alternative radiopacifiers for polymethyl methacrylate bone cements: silane-treated anatase titanium dioxide and yttria-stabilised zirconium dioxide, J Biomater Appl. 35 (2021) 1235–1252.
[9] S. Brandriss, S. Margel, Synthesis and characterization of self-assembled hydrophobic monolayer coatings on silica colloids, Langmuir 9 (1993) 1232–1240.
[10] W.N. Ayre, T. Scott, K. Hallam, A.W. Blom, S. Denyer, H.K. Bone, J.P. Mansell, Fluorophosphonate-functionalised titanium via a pre-adsorbed alkane phosphonic acid: a novel dual action surface finish for bone regenerative applications, J. Mater. Sci. - Mater. Med. 27 (2015) 36.
[11] W. Zhao, M. Göthelid, S. Hosseinpour, M.B. Johansson, G. Li, C. Leygraf, C. M. Johnson, The nature of self-assembled octadecylphosphonic acid (ODPA) layers on copper substrates, J. Colloid Interface Sci. 581 (2021) 816–825.
[12] I.L. Liakos, R.C. Newman, E. McAlpine, M.R. Alexander, Study of the resistance of SAMs on aluminium to acidic and basic solutions using dynamic contact angle measurement, Langmuir 23 (2007) 995–999.
[13] T. Hauffman, O. Blajiev, J. Snauwaert, C. van Haesendonck, A. Hubin, H. Terryn, Study of the self-assembling of n-octylphosphonic acid layers on aluminum oxide, Langmuir 24 (2008) 13450–13456.
[14] R. Bhure, T.M. Abdel-Fattah, C. Bonner, F. Hall, A. Mahapatro, Stability of phosphonic self assembled monolayers (SAMs) on cobalt chromium (Co–Cr) alloy under oxidative conditions, Appl. Surf. Sci. 257 (2011) 5605–5612.
[15] A. Kanta, R. Sedev, J. Ralston, The formation and stability of self-assembled monolayers of octadecylphosphonic acid on titania, Colloids Surf., A 291 (2006) 51–58.
[16] X. Chen, E. Luais, N. Darwish, S. Ciampi, P. Thordarson, J.J. Gooding, Studies on the effect of solvents on self-assembled monolayers formed from organophosphonic acids on indium tin oxide, Langmuir 28 (2012) 9487–9495.
[17] A. Roevens, J.G. Van Dijck, M. Tassi, J. D’Haen, R. Carleer, P. Adriaensens, F. Blockhuys, V. Meynen, Revealing the influence of the solvent in combination

with temperature, concentration and pH on the modification of TiO_2 with 3PA, Mater. Chem. Phys. 184 (2016) 324–334.
[18] D. Chen, H.K. Yin Wu, S. Naderi-Gohar, Y. Wu, Y. Huang, H.-Y. Nie, An extremely rapid dip-coating method for self-assembly of octadecylphosphonic acid and its thermal stability on an aluminum film, J. Mater. Chem. C 2 (2014) 9941–9948.
[19] H.-Y. Nie, Revealing different bonding modes of self-assembled octadecylphosphonic acid monolayers on oxides by time-of-flight secondary ion mass spectrometry: silicon vs aluminum, Anal. Chem. 82 (2010) 3371–3376.
[20] H.-Y. Nie, Self-assembled monolayers of octadecylphosphonic acid and polymer films: surface chemistry and chemical structures studied by time-of-flight secondary ion mass spectrometry, Surf. Interface Anal. 49 (2017) 1431–1441.
[21] H.-Y. Nie, M.J. Walzak, N.S. McIntyre, Delivering octadecylphosphonic acid self-assembled monolayers on a Si wafer and other oxide surfaces, J. Phys. Chem. B 110 (2006) 21101–21108.
[22] E.S. Gawalt, K. Brault-Rios, M.S. Dixon, D.C. Tang, J. Schwartz, Enhanced bonding of organometallics to titanium via a titanium(III) phosphate interface, Langmuir 17 (2001) 6743–6745.
[23] E.S. Gawalt, M.J. Avaltroni, N. Koch, J. Schwartz, Self-assembly and bonding of alkanephosphonic acids on the native oxide surface of titanium, Langmuir 17 (2001) 5736–5738.
[24] G. Sauerbrey, Verwendung von Schwingquarzen zur Wägung dünner Schichten und zur Mikrowägung, Z. Phys. 155 (1959) 206–222.
[25] N. Fairley, V. Fernandez, M. Richard-Plouet, C. Guillot-Deudon, J. Walton, E. Smith, D. Flahaut, M. Greiner, M. Biesinger, S. Tougaard, D. Morgan, J. Baltrusaitis, Systematic and collaborative approach to problem solving using X-ray photoelectron spectroscopy, Appl. Surf. Sci. Adv. 5 (2021) 100112.
[26] L.R. Azizova, T.V. Kulik, B.B. Palianytsia, G.M. Telbiz, M.T. Kartel, Secondary structure of muramyl dipeptide glycoside in pristine state and immobilized on nanosilica surface, Colloids Surf., A 631 (2021) 127724.
[27] L.R. Azizova, T.V. Kulik, B.B. Palianytsia, A.E. Zemlyakov, V.N. Tsikalova, V. Y. Chirva, Investigation of chemical transformations of thiophenylglycoside of muramyl dipeptide on the fumed silica surface using TPD-MS, FTIR spectroscopy and ES IT MS, Nanoscale Res. Lett. 9 (2014) 234.
[28] L.R. Azizova, T.V. Kulik, B.B. Palianytsia, N.A. Lipkovska, Thermal and hydrolytic stability of grafted ester groups of carboxylic acids on the silica surface, J. Therm. Anal. Calorim. 122 (2015) 517–523.
[29] T. Kulik, B. Palianytsia, M. Larsson, Catalytic pyrolysis of aliphatic carboxylic acids into symmetric ketones over ceria-based catalysts: kinetics, Isotope Effect Mech. Catal. 10 (2020) 179.
[30] K. Kulyk, V. Ishchenko, B. Palyanytsya, V. Khylya, M. Borysenko, T. Kulyk, A TPD-MS study of the interaction of coumarins and their heterocyclic derivatives with a surface of fumed silica and nanosized oxides CeO_2/SiO_2, TiO_2/SiO_2, Al_2O_3/SiO_2, J. Mass Spectrom. 45 (2010) 750–761.
[31] K. Kulyk, M. Borysenko, T. Kulik, L. Mikhalovska, J.D. Alexander, B. Palianytsia, Chemisorption and thermally induced transformations of polydimethylsiloxane on the surface of nanoscale silica and ceria/silica, Polym. Degrad. Stab. 120 (2015) 203–211.
[32] K. Kulyk, H. Zettergren, M. Gatchell, J.D. Alexander, M. Borysenko, B. Palianytsia, M. Larsson, T. Kulik, Dimethylsilanone generation from pyrolysis of polysiloxanes filled with nanosized silica and ceria/silica, ChemPlusChem 81 (2016) 1003–1013.
[33] E.S. Gawalt, M.J. Avaltroni, M.P. Danahy, B.M. Silverman, E.L. Hanson, K. S. Midwood, J.E. Schwarzbauer, J. Schwartz, Bonding organics to Ti alloys: facilitating human osteoblast attachment and spreading on surgical implant materials, Langmuir 19 (2003) 200–204.
[34] J. Schwartz, M.J. Avaltroni, M.P. Danahy, B.M. Silverman, E.L. Hanson, J. E. Schwarzbauer, K.S. Midwood, E.S. Gawalt, Cell attachment and spreading on metal implant materials, Mater. Sci. Eng., C 23 (2003) 395–400.
[35] S. Kravchenko, B. Snopok, "Vanishing mass" in the Sauerbrey world: quartz crystal microbalance study of self-assembled monolayers based on a tripod-branched structure with tuneable molecular flexibility, Analyst 145 (2020) 656–666.
[36] P. Castro, P. Resa, L. Elvira, Apparent negative mass in QCM sensors due to punctual rigid loading, IOP Conf. Ser.: Mater. Sci. Eng. 42 (2012) 012046.
[37] G. Mani, D.M. Johnson, D. Marton, V.L. Dougherty, M.D. Feldman, D. Patel, A. A. Ayon, C.M. Agrawal, Stability of self-assembled monolayers on titanium and gold, Langmuir 24 (2008) 6774–6784.
[38] R. Hofer, M. Textor, N.D. Spencer, Alkyl phosphate monolayers, self-assembled from aqueous solution onto metal oxide surfaces, Langmuir 17 (2001) 4014–4020.
[39] D. Brovelli, G. Hähner, L. Ruiz, R. Hofer, G. Kraus, A. Waldner, J. Schlösser, P. Oroszlan, M. Ehrat, N.D. Spencer, Highly oriented, self-assembled alkanephosphate monolayers on tantalum(V) oxide surfaces, Langmuir 15 (1999) 4324–4327.
[40] C. Messerschmidt, D.K. Schwartz, Growth mechanisms of octadecylphosphonic acid self-assembled monolayers on sapphire (corundum): evidence for a quasi-equilibrium triple point, Langmuir 17 (2001) 462–467.
[41] E. Hoque, J.A. DeRose, G. Kulik, P. Hoffmann, H.J. Mathieu, B. Bhushan, Alkylphosphonate modified aluminum oxide surfaces, J. Phys. Chem. B 110 (2006) 10855–10861.
[42] E. McCafferty, J.P. Wightman, Determination of the concentration of surface hydroxyl groups on metal oxide films by a quantitative XPS method, Surf. Interface Anal. 26 (1998) 549–564.
[43] G. Zorn, I. Gotman, E.Y. Gutmanas, R. Adadi, G. Salitra, C.N. Sukenik, Surface modification of Ti45Nb alloy with an alkylphosphonic acid self-assembled monolayer, Chem. Mater. 17 (2005) 4218–4226.
[44] A.Y. Fadeev, R. Helmy, S. Marcinko, Self-assembled monolayers of organosilicon hydrides supported on titanium, zirconium, and hafnium dioxides, Langmuir 18 (2002) 7521–7529.
[45] X. Wan, I. Lieberman, A. Asyuda, S. Resch, H. Seim, P. Kirsch, M. Zharnikov, Thermal stability of phosphonic acid self-assembled monolayers on alumina substrates, J. Phys. Chem. C 124 (2020) 2531–2542.
[46] K. Kulyk, B. Palianytsia, J.D. Alexander, L. Azizova, M. Borysenko, M. Kartel, M. Larsson, T. Kulik, Kinetics of valeric acid ketonization and ketenization in catalytic pyrolysis on nanosized SiO_2, γ-Al_2O_3, CeO_2/SiO_2, Al_2O_3/SiO_2 and TiO_2/SiO_2, ChemPhysChem 18 (2017) 1943–1955.
[47] N. Nastasiienko, T. Kulik, B. Palianytsia, J. Laskin, T. Cherniavska, M. Kartel, M. Larsson, Catalytic pyrolysis of lignin model compounds (pyrocatechol, guaiacol, vanillic and ferulic acids) over nanoceria catalyst for biomass conversion, Appl. Sci. 11 (2021) 7205.
[48] T. Kulik, N. Nastasiienko, B. Palianytsia, M. Ilchenko, M. Larsson, Catalytic pyrolysis of lignin model compound (ferulic acid) over alumina: surface complexes, kinetics, and mechanisms, Catalysts 11 (2021) 1508.
[49] M.U. Kislyuk, V.V. Rozanov, Temperature-programmed desorption and temperature-programmed reaction as methods for studying the kinetics and mechanism of heterogeneous catalytic processes, Kinet. Catal. 36 (1995) 80–88.
[50] L.D.S. Yadav, Mass Spectroscopy (MS), in: O. Spectroscopy (Ed.), Springer, Dordrecht, Netherlands, 2005, pp. 250–294.
[51] M.E. Skindersoe, K.A. Krogfelt, A. Blom, G. Jiang, G.D. Prestwich, J.P. Mansell, Dual action of lysophosphatidate-functionalised titanium: interactions with human (MG63) osteoblasts and methicillin resistant staphylococcus aureus, PLoS ONE 10 (2015) e0143509.
[52] K.M. Wiencek, M. Fletcher, Bacterial adhesion to hydroxyl- and methyl-terminated alkanethiol self-assembled monolayers, J. Bacteriol. 177 (1995) 1959–1966.
[53] N. Cerca, G.B. Pier, M. Vilanova, R. Oliveira, J. Azeredo, Quantitative analysis of adhesion and biofilm formation on hydrophilic and hydrophobic surfaces of clinical isolates of Staphylococcus epidermidis, Res. Microbiol. 156 (2005) 506–514.
[54] Y.H. An, R.J. Friedman, Concise review of mechanisms of bacterial adhesion to biomaterial surfaces, J. Biomed. Mater. Res. 43 (1998) 338–348.
[55] K.M. Wiencek, M. Fletcher, Effects of substratum wettability and molecular topography on the initial adhesion of bacteria to chemically defined substrata, Biofouling 11 (1997) 293–311.
[56] M.G. Katsikogianni, Y.F. Missirlis, Bacterial adhesion onto materials with specific surface chemistries under flow conditions, J. Mater. Sci. - Mater. Med. 21 (2010) 963–968.